Structural, magnetic, and electronic properties of Ni_n and Fe_n nanostructures ($n=1-4$) adsorbed on zigzag graphene nanoribbons

R. C. Longo,[1] J. Carrete,[1] J. Ferrer,[2] and L. J. Gallego[1]
[1]*Departamento de Física de la Materia Condensada, Facultad de Física, Universidad de Santiago de Compostela, E-15782 Santiago de Compostela, Spain*
[2]*Departamento de Física, Universidad de Oviedo, E-33007 Oviedo, Spain*
(Received 19 October 2009; revised manuscript received 5 February 2010; published 11 March 2010)

Extensive *ab initio* density-functional calculations were performed to investigate the structural, magnetic, and electronic properties of systems comprising Ni_n and Fe_n nanostructures ($n=1-4$) adsorbed on hydrogen-passivated zigzag graphene nanoribbons (GNRs). Both Ni and Fe atoms were most strongly bound at GNR edge sites and neither altered whether the GNR was metallic or semiconducting. However, Ni_n nanostructures were more strongly bound than Fe_n nanostructures, and their atoms had much smaller spin magnetic moments; Ni_n/GNR systems, like the pristine GNR, always had lowest energy with antiparallel edge spins, whereas among Fe_n/GNR systems this was only found for one- or two-atom adstructures at subedge or near-subedge atop sites; and zigzag Ni_3 and Ni_4 chains placed at GNR hole sites retained close contact with the GNR upon relaxation, whereas the analogous Fe chains adopted geometries similar to those of free-standing Fe clusters, with one or more atoms lifted away from the GNR.

DOI: 10.1103/PhysRevB.81.115418 PACS number(s): 73.22.−f, 71.15.Mb, 71.15.Dx

I. INTRODUCTION

Identification of Kroto *et al.*[1] of the truncated icosahedral structure of C_{60} in 1985 spurred intense research on the properties of fullerenes and other all-carbon nanostructures, especially carbon nanotubes (CNTs)[2,3] and the graphene sheet.[4–9] The latter is a zero-gap two-dimensional semiconductor with striking properties of interest for nanoelectronics; in particular, it has extremely high carrier mobility due to the linear band dispersion around the Fermi point.[5] CNTs, obtained conceptually by rolling up a strip of graphene sheet, are uniquely specified by their diameter and winding angle, which together determine not only their structure but also other properties, such as whether they behave electronically as conductors or semiconductors.[3] A carbon nanostructure that has attracted considerable attention of late is the graphene nanoribbon (GNR), an (unrolled) graphene strip.[10–31] Just as the structures and electronic properties of CNTs are determined by their diameter and winding angle, so those of GNRs are determined by their width and by the direction-dependent configuration of atoms along their long edges, which can range from zigzag (the edges run perpendicular to one of the bond directions) to armchair (the edges run parallel to one of the bond directions). In particular, zigzag GNRs with hydrogen-passivated edges, in which all the spins are the same along each edge, are metallic or semiconducting depending on whether the two edges have the same or opposite spins[24] [the latter configuration, Ferro-A, is marginally more stable than the former, Ferro-F, in which antiferromagnetic (AFM) coupling between nearest neighbors is frustrated at the center of the ribbon].[17,29]

CNTs can be obtained with the catalytic aid of late transition metals (TMs), notably Ni.[3,32–34] For this and other reasons, there has been considerable research on nanostructures composed of C and TM atoms. It is found, for example, that systems with early TMs differ markedly from those with late TMs. Thus early TMs do not catalyze CNT formation, and early $3d$ metals (Ti, V, and Cr) preferentially form "met-cars"[35–41] (clusters with TM_8C_{12} stoichiometry and remarkable stability), while late $3d$ metals (Co and Ni) do not.[41] Knowledge of how TM-C interactions depend on where the TM atoms bind is of fundamental importance for understanding not only catalytic CNT growth, the mechanism of which is still controversial,[33,42] but also the magnetic and other electronic properties of carbon nanostructures with adsorbed or embedded TM atoms. For example, GAUSSIAN03[43] calculations have predicted that the electron tunneling current in Ni-C_{60}-Ni is greater when the Ni atoms occupy hole sites than in the more stable structure[44] in which they occupy bridge sites.[45] Of course, non-TM atoms can also alter electronic properties: hydrogen-passivated zigzag GNRs with boron-doped ferromagnetically coupled edges have been shown theoretically to be semiconductors with spin-sensitive transmittance.[24]

Ab initio calculations using SIESTA[46] and TRANSAMPA[47] have shown that the most stable configuration of a hydrogen-passivated zigzag GNR with a single adsorbed Ni atom features the adatom at an edge site, that the adsorption process reduces the magnetic moments of both the Ni and its neighboring C atoms due to the hybridization of Ni $3d$ orbitals with C $2p$ orbitals, and that the electronic transmittance along the GNR is, as in the case of B-doped zigzag GNRs,[24] spin dependent.[29] To contribute to a better understanding of the behavior of TM/GNR systems, in the work described here we performed SIESTA calculations to compare the structural, magnetic, and electronic behaviors of Ni_n and Fe_n structures ($n=1-4$) that were supported on hydrogen-passivated zigzag GNRs. The Ni_n/GNR and Fe_n/GNR systems proved to differ significantly in many respects. The essential technical details of the method used are sketched in Sec. II, our results are discussed in Sec. III, and in Sec. IV we summarize our main conclusions.

II. DETAILS OF THE COMPUTATIONAL PROCEDURE

The computational method employed has been described in detail in Ref. 46. Briefly, it is a density-functional

theory (DFT) approach using numerical pseudoatomic orbitals as basis sets to solve the single-particle Kohn-Sham equations. For the exchange and correlation potential we used the Perdew-Burke-Ernzerhof form of the generalized gradient approximation (GGA).[48] The atomic cores were described by nonlocal norm-conserving Troullier-Martins pseudopotentials[49] factorized in the Kleinman-Bylander form.[50] The pseudopotentials for Ni and Fe were generated using the valence configurations $4s^1 3d^9$ and $4s^1 3d^7$ and have been validated in previous work on Ni-C and Fe-C clusters.[51–53] For both TM and C atoms, valence states were described using triple-ζ doubly polarized basis sets. The energy cutoff used to define the real-space grid for the numerical calculations involving the electron density was 250 Ry (in a few calculations performed as a check with a 500 Ry energy cutoff, the results were virtually the same as those obtained with the smaller cutoff). Using a conjugate gradient method,[54] all the structures were fully relaxed, without any geometry or spin constraints, until the interatomic forces were smaller than 0.005 eV/Å.

Most calculations concerned a $9.83 \times 50 \times 10$ Å supercell containing four unit cells of a hydrogen-passivated $\langle 10,0 \rangle$ zigzag GNR (80 C atoms together with 8 H atoms saturating the dangling σ bonds at the edges)[55] together with Ni or Fe adatoms. Periodic boundary conditions were applied in all directions to make infinite copies of an endless adatom-spattered GNR 22.08 Å wide in the y direction, with copies separated by 10 and 50 Å in the z and y directions, respectively. For the largest TM nanostructures, eight unit cells of GNR were included in the supercell as a check on accuracy. For some TM nanostructures, calculations were also performed in which the dangling σ bonds were passivated with alternating H atoms and methylene groups,[17] but the results were the same as with H-only passivation. A Monkhorst-Pack[56] grid of $9 \times 1 \times 1$ k points was used along the GNR growth direction (x direction) for integration in the Brillouin zone; calculations performed with a $15 \times 1 \times 1$ grid gave virtually the same results.

III. RESULTS AND DISCUSSION

We started our calculations by reproducing known results for pristine hydrogen-passivated zigzag GNRs, i.e., zigzag GNRs with no TM atoms. We found the energy of Ferro-A to be just 0.014 eV/unit cell lower than that of Ferro-F. Note that Pisani *et al.*[17] showed that although different exchange and correlation functionals can afford slightly different predictions of the magnetic configuration of GNRs, the qualitative features of the results are robust with respect to changes of functional. This should also hold for the results obtained in this paper for Ni_n/GNR and Fe_n/GNR systems.

Following the above preliminaries, we performed extensive calculations on single-adatom Ni/GNR and Fe/GNR systems to investigate, as possible adsorption sites, the central hole site (CHS) of the GNR unit cell, a subcentral bridge site (SCBS), and a subedge "atop" site (SEAS) [see Figs. 1(a)–1(c)]. In each case, we also investigated magnetic behavior; magnetic differences between the Ni/GNR and Fe/GNR systems were expected because the Fe atom has three unpaired d electrons and the Ni atom has only one. Due to space limitations, we present here only part of our results for these and other Ni_n/GNR and Fe_n/GNR systems ($n=2-4$); for the remainder, see the supplementary material.[57]

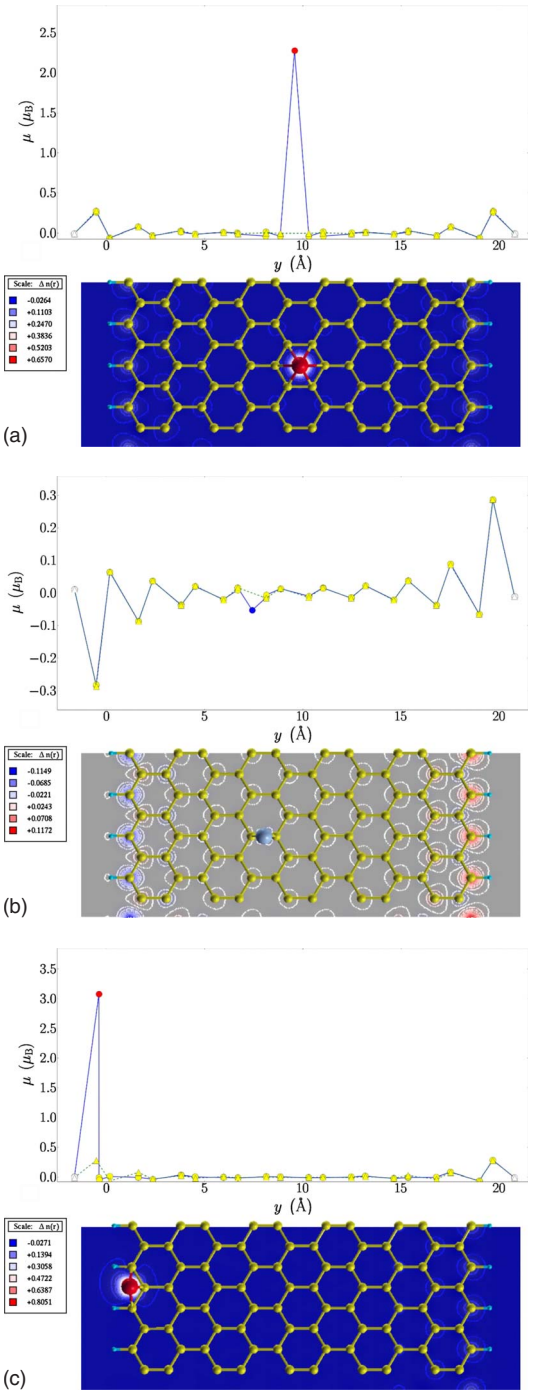

FIG. 1. (Color online) Lower panels: spin density distributions of the systems (a) Fe(CHS)/Ferro-F, (b) Ni(SCBS)/Ferro-A, and (c) Fe(SEAS)/Ferro-F after full relaxation, calculated by taking the difference between the spin-up and spin-down densities and integrating along the z direction (Ref. 59). Upper panels: spin magnetic moments of all atoms in a band perpendicular to the x axis which contains the adatom (white, hydrogen; yellow, carbon; red, Fe; and blue, Ni; triangles and dashed lines correspond to pristine GNR and circles and continuous lines correspond to TM/GNR).

TABLE I. Nomenclature employed in this paper for Ni_n adstructures ($n=1-4$) on a $\langle 10,0\rangle$ GNR in Ferro-A and Ferro-F configurations, together with the absolute values of the adsorption energies, and the magnetic moments of the Ni atoms and of two C atoms at opposite edges of the ribbon. Names indicate initial geometries: CHS, central hole site; SCBS, subcentral bridge site; SEAS, subedge atop site; NHS, neighboring hole site; DD, double decker (one adatom atop another); NAS, neighboring atop site; 2SEAS, SEAS+SEAS; CHS-LC, linear chain starting at CHS; and CHS-ZZC, zigzag chain starting at CHS.

		E (eV)		μ_{Ni} (μ_B)		μ_C (μ_B)	
n	Name	Ferro-A	Ferro-F	Ferro-A	Ferro-F	Ferro-A	Ferro-F
1	CHS	1.611	1.592	0.00	−0.03	−0.285, 0.285	0.276, 0.276
	SCBS	1.297	1.276	−0.05	0.10	−0.283, 0.287	0.282, 0.286
	SEAS	1.978	1.965	−0.51	0.47	−0.113, 0.286	0.104, 0.280
2	CHS+NHS	3.753	3.733	−0.012, 0.0	−0.023, −0.026	−0.284, 0.282	0.276, 0.275
	DD-CHS	3.977	3.902	−1.305, −0.653	1.287, 0.761	−0.286, 0.286	0.285, 0.284
	SEAS+NAS	4.283	4.266	−0.42, −0.44	0.42, 0.36	−0.105, 0.286	0.098, 0.280
	DD-SEAS	4.560	4.553	1.173, 0.097	1.172, 0.11	−0.077, 0.286	0.08, 0.286
	2SEAS	4.705	4.689	−0.197, −0.763	0.169, 0.705	−0.028, 0.288	0.022, 0.283
3	CHS-LC	5.769	5.756	−0.01, −0.001, 0.009	0.002, −0.094, 0.002	−0.281, 0.281	0.275, 0.276
	CHS-ZZC	5.843	5.827	−0.085, −0.013, 0.04	0.035, −0.012, −0.017	−0.281, 0.283	0.271, 0.279
4	CHS-LC	7.840	7.829	−0.010, −0.040, −0.009, 0.004	0.027, 0.100, 0.107, 0.048	−0.273, 0.283	0.283, 0.272
	CHS-ZZC	9.751	9.699	−0.492, −0.598, 0.590, 0.481	0.473, 0.613, 0.579, 0.477	−0.284, 0.282	0.288, 0.277

The entries for $n=1$ in Tables I and II list the predicted adsorption energies of Ni and Fe on Ferro-A and Ferro-F, together with the spin magnetic moments of the adatom and of the nearest C atoms of the two edges (for each n, magnetic moments were in fact calculated for all atoms in a band perpendicular to the x direction that contained the adatoms). For both metals, the most stable structure featured the adatom at a Ferro-A SEAS, which in the case of Ni/GNR agrees with the results of Rigo *et al.*[29] Unlike Rigo *et al.*, however, we found that adsorption at an SCBS was also stable for Ni [Ni(SCBS)/Ferro-A being slightly more stable than Ni(SCBS)/Ferro-F] though not for Fe. This result for Ni is consistent with the stability of C_{60} with Ni adsorbed at bridge sites.[44,45] When adsorption occurred at the CHS, Ni(CHS)/Ferro-A was again slightly more stable than Ni(CHS)/Ferro-F, but adsorption of Fe reversed the spin preference of the pristine GNR, Fe(CHS)/Ferro-F being much more stable than Fe(CHS)/Ferro-A. For all configura-

TABLE II. As for Table I but for Fe_n adstructures ($n=1-4$). For Fe_3/Ferro-F and Fe_4/Ferro-F, we also include results for SEAS-ZZCs (ZZCs that started at a SEAS and continued toward the center of the GNR; see text).

		E (eV)		μ_{Fe} (μ_B)		μ_C (μ_B)	
n	Name	Ferro-A	Ferro-F	Ferro-A	Ferro-F	Ferro-A	Ferro-F
1	CHS	0.074	0.607	−0.75	2.27	−0.286, 0.286	0.272, 0.272
	SCBS	Unstable					
	SEAS	1.043	1.036	−3.08	3.07	−0.021, 0.284	0.012, 0.282
2	CHS+NHS	1.987	2.550	3.037, −3.087	3.521, 3.191	−0.276, 0.282	0.258, 0.274
	DD-CHS	2.955	2.974	−3.021, −3.288	3.013, 3.281	−0.278, 0.280	0.275, 0.280
	SEAS+NAS	3.348	3.324	−3.396, −3.432	3.398, 3.422	−0.106, 0.288	0.095, 0.286
	DD-SEAS	3.519	3.503	−2.410, −3.214	2.397, 3.206	−0.139, 0.286	0.146, 0.284
	2SEAS	3.571	3.542	−3.443, −3.438	3.448, 3.442	−0.068, 0.29	0.07, 0.288
3	CHS-LC	3.415	3.752	3.402, −2.273, 3.398	2.828, 3.261, 2.79	−0.279, 0.252	0.264, 0.265
	CHS-ZZC	4.734	5.524	−3.156, −0.084, 3.306	2.8, 3.017, 2.805	−0.276, 0.279	0.263, 0.282
	SEAS-ZZC		6.180		2.933, 3.050, 2.970		0.032, 0.281
4	CHS-LC	4.712	5.064	−3.075, −3.459, 3.463, 2.990	3.509, 3.207, 3.130, 3.497	−0.266, 0.252	0.263, 0.248
	CHS-ZZC	7.537	8.411	−2.700, −2.729, 2.941, 2.331	3.350, 2.871, 2.878, 3.302	−0.263, 0.282	0.262, 0.281
	SEAS-ZZC		8.646		3.125, 3.302, 3.016, 3.342		0.003, 0.286

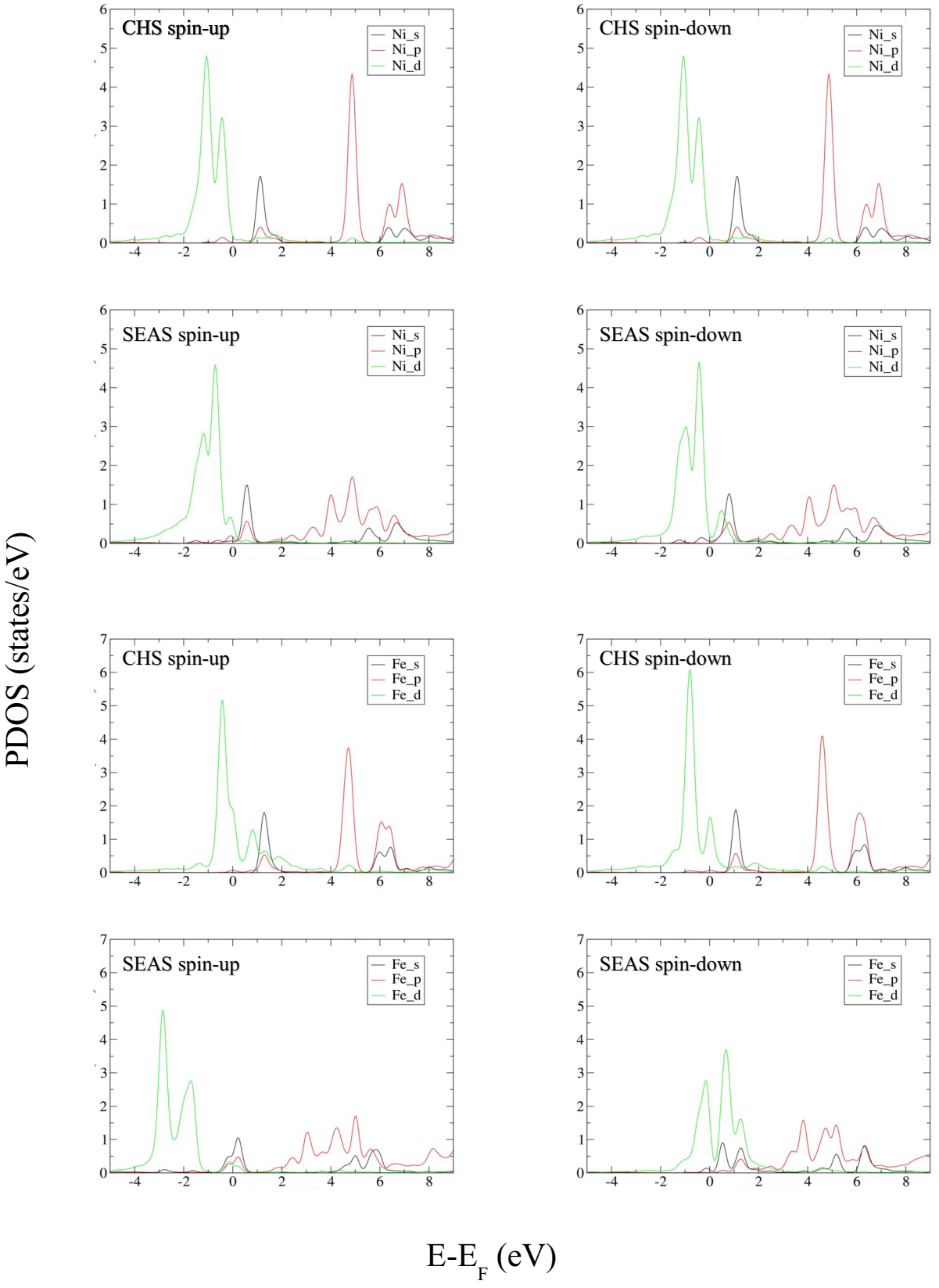

FIG. 2. (Color online) Ni and Fe PDOSs of TM(CHS)/Ferro-A and TM(SEAS)/Ferro-A (TM=Ni,Fe). The PDOS delta functions have been replaced by Gaussian functions of finite breadth.

tions, the Fe/GNR was less stable than the Ni/GNR, a finding that was repeated for $n=2$, 3, and 4 and which is in keeping with results for TM adsorption on graphene.[58]

Figures 1(a)–1(c) show the spin density and magnetic moment results for Fe(CHS)/Ferro-F, Ni(SCBS)/Ferro-A, and Fe(SEAS)/Ferro-F, respectively, after full relaxation; the re-

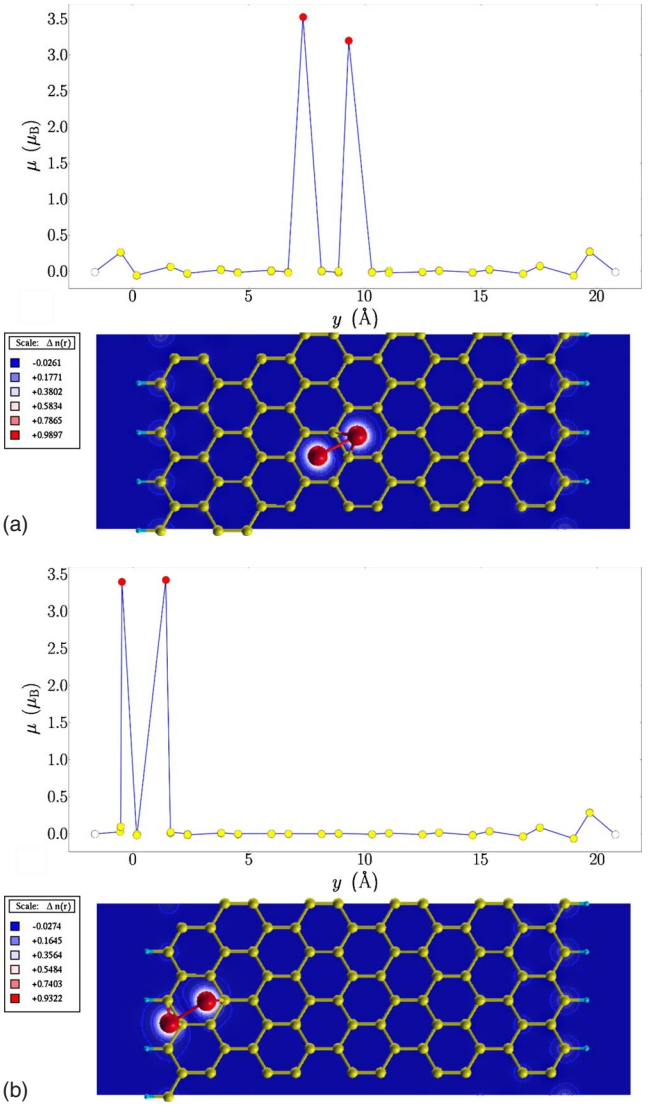

FIG. 3. (Color online) As for Fig. 1, but for (a) Fe_2(CH+NHS)/Ferro-F and (b) Fe_2(SEAS+NAS)/Ferro-F.

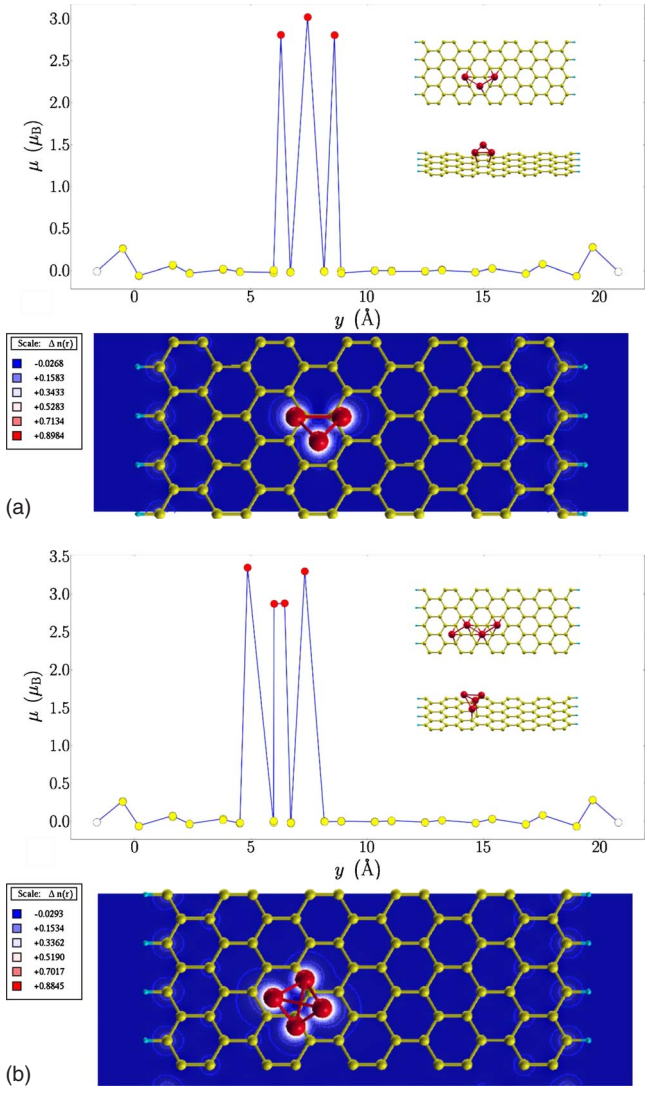

FIG. 4. (Color online) As for Fig. 1, but for (a) Fe_3(CHS-ZZC)/Ferro-F and (b) Fe_4(CHS-ZZC)/Ferro-F. Insets show the initial structures together with side views of those obtained upon full relaxation.

maining results are included in the supplementary material.[57] At the CHS, the magnetic moment of the Ni atom in Ni(CHS)/Ferro-A was zero due to hybridization between the Ni $3d$ and nearest-neighbor C $2p$ orbitals, although in the less stable Ni(CHS)/Ferro-F it had a small magnetic moment with AFM coupling to the edge C atoms (see Table I). By contrast, the Fe atom had an appreciable magnetic moment in both Fe(CHS)/Ferro-A and Fe(CHS)/Ferro-F [see Table II and Fig. 1(a)], with ferromagnetic (FM) coupling to the edge C atoms in the latter. The energetic disadvantage of Fe(CHS)/Ferro-A would seem to be due to the Fe atom not being able to couple ferromagnetically to both edges; of course, no such frustration can occur in Ni(CHS)/Ferro-A, in which the magnetic moment of the Ni atom is zero. At an SCBS, an Ni adatom had a slightly larger magnetic moment than at the CHS due to a lesser degree of hybridization and coupled ferromagnetically to the nearest edge in both Ni(SCBS)/Ferro-A and Ni(SCBS)/Ferro-F [see Table I and Fig. 1(b)]; however, both these structures were less stable than their CHS analogs. The most stable single-adatom configurations featured the Ni or Fe atoms at SEAS, and in both cases Ferro-A was just marginally more stable than Ferro-F. The magnetic moments of Ni in Ni(SEAS)/Ferro-A and Ni(SEAS)/Ferro-F, $0.51\mu_B$ and $0.47\mu_B$, respectively, are in keeping with the values predicted by Rigo *et al.*,[29] $0.53\mu_B$ and $0.47\mu_B$. The stronger magnetic character of Fe is reflected by magnetic moments of $3.08\mu_B$ in Fe(SEAS)/Ferro-A and $3.07\mu_B$ in Fe(SEAS)/Ferro-F [see Table II and Fig. 1(c)].

Figure 2 shows the projected density of states (PDOS) of Ni and Fe atoms adsorbed on Ferro-A at the CHS and at a SEAS. At the CHS, the Ni PDOS below the Fermi level E_F is composed of d-type states resulting from hybridization between the $3d$ orbitals of the Ni adatom and the nearest-neighbor C $2p$ orbitals, which lowers the lower limit of the effective d band to approximately 4 eV below E_F. Equal spin-up and spin-down densities give a zero spin magnetic moment. At the SEAS, there are unoccupied spin-down

d-type states in an energy range of about 0–2 eV above E_F, in consonance with the nonzero spin magnetic moment of the Ni adatom at this position. Moreover, the unoccupied *p* orbitals are now delocalized π^* orbitals. When the adatom is Fe at the CHS, delocalized unoccupied π^* orbitals are accompanied by significant unoccupied spin-up and spin-down *d*-type state densities around 0.8 and 0.0 eV above E_F, respectively, while at the SEAS the two main *d*-type peaks of the spin-up and spin-down densities are located within windows about 2 eV wide around 2.4 and 0 eV below E_F, respectively.

The five two-adatom configurations investigated had adatoms at the CHS and at a neighboring hole site closer to one of the edges of the ribbon (CHS+NHS), at a SEAS and a neighboring atop site closer to the center of the ribbon (SEAS+NAS), at two neighboring SEAS (2SEAS), at a single SEAS, in a double-decker configuration with one of the two adatoms atop the other (DD-SEAS), and in a similar double-decker configuration at the CHS (DD-CHS). These last two configurations were included to allow comparison with the finding of Johll *et al.*[58] that TM dimers on graphene bind most stably in DD-CHS-like configurations. Tables I and II list postrelaxation energies and the spin magnetic moments of adatoms and edge carbons, and Figs. 3(a) and 3(b) show spin density and magnetic moment results for Fe_2(CHS+NHS)/Ferro-F and Fe_2(SEAS+NAS)/Ferro-F (the remainder are included in the supplementary material[57]). In all five Ni pair configurations, the Ferro-A configuration of the GNR was slightly more stable than the Ferro-F configuration. In the CHS+NHS configuration, both Ni atoms behaved similarly to single Ni atoms at the CHS, with zero or very small magnetic moments; in the SEAS+NAS configuration, both had appreciable magnetic moments (though somewhat smaller than those of a solitary Ni atom at a SEAS), while in the 2SEAS configuration (the most stable), one of the Ni atoms had a larger magnetic moment than in the SEAS+NAS configuration ($\approx 0.7\mu_B$) and the other had a smaller (note that the 2SEAS configuration did not lie parallel to the *x* axis after full relaxation). The double-decker configuration DD-CHS was somewhat more stable than CHS+NHS, but DD-SEAS was less stable than 2SEAS (though more so than SEAS+NAS). In both the double-decker configurations, the top adatom retained more than half the magnetic moment of the isolated Ni atom ($2\mu_B$), but the bottom adatom did not.

When the two adatoms were Fe, the Ferro-A configuration of the GNR was marginally the more stable with the Fe pair in the configurations SEAS+NAS, DD-SEAS and 2SEAS, but the reverse held for DD-CHS, and Fe_2(CHS+NHS)/Ferro-F was about 0.5 eV more stable than Fe_2(CHS+NHS)/Ferro-A. The stabilities of the various configurations increased in the same order as for Ni: CHS + NHS < DD-CHS < SEAS + NAS < DD-SEAS < 2 SEAS, though the energy difference between these last two was much smaller than for the Ni analogs. In CHS+NHS configuration, both Fe atoms had magnetic moments $>3.0\mu_B$ [one had a magnetic moment as large as $3.521\mu_B$ in Fe_2(CHS+NHS)/Ferro-F], and the greater stability of the Ferro-F configuration is attributable to both its Fe atoms coupling ferromagnetically to the edge carbons, whereas in

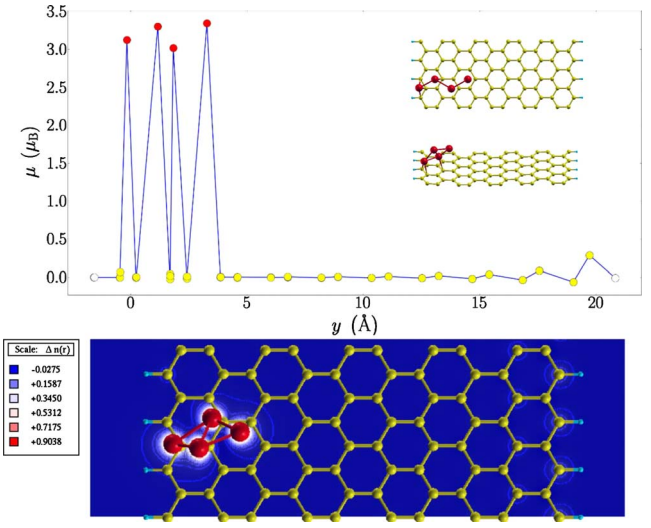

FIG. 5. (Color online) As for Fig. 4, but for Fe_4(SEAS-ZZC)/Ferro-F.

Fe_2(CHS+NHS)/Ferro-A there is FM coupling between the CHS atom and one edge, and AFM coupling between this atom and the other edge, between the NHS atom and its nearest edge, and between the two Fe atoms. In the SEAS +NAS configuration, both Fe atoms had magnetic moments of about $3.4\mu_B$ regardless of the GNR configuration, and in the 2SEAS configuration (the most stable), both always had magnetic moments of about $3.44\mu_B$. The magnetic moments of the two adatoms in the double-decker configurations were much more similar than in the case of Ni, but differed more than in the other configurations (by $0.8\mu_B$ in DD-SEAS).

Note that in DD-CHS configuration, both Ni_2/Ferro-F and Fe_2/Ferro-F had adsorption energies and magnetic moments similar to those reported for a double-decker configuration at a hole site of graphene: 3.58 eV, $1.29\mu_B$ and $0.73\mu_B$ for Ni, and 3.0 eV, $3.48\mu_B$ and $2.76\mu_B$ for Fe.[58]

The three- and four-adatom configurations investigated were, before relaxation, linear and zigzag chains (LCs and ZZCs) with an atom at the CHS and the other atoms at neighboring hole sites or (for Fe ZZCs) an atom at a SEAS and the other atoms at atop sites nearer the center of the GNR [see Figs. 4(a), 4(b), and 5 and the supplementary material[57]]. Ferromagnetically coupled ZZCs are the most stable configurations of free-standing Ni and Fe chains of infinite length.[60] Note that, in view of the preference of Fe and Ni dimers for the 2SEAS configuration, none of the three- or four-adatom structures studied is likely to be the ground state structure for that number of adatoms. It seems probable that the adatoms of the ground state structures all occupy SEASs, and for a study of such structures to prevent interactions between the adstructure and its images in neighboring supercells it would be necessary to use a supercell much larger than four unit cells. The structures we were able to examine in the present study nevertheless enable comparison between LCs and ZZCs and between Fe ZZCs in more central and more lateral locations, as well as comparison of Fe with Ni. Tables I and II list postrelaxation energies and spin magnetic moments, and Figs. 4(a), 4(b), and 5 show spin densities and magnetic moments across the GNR for

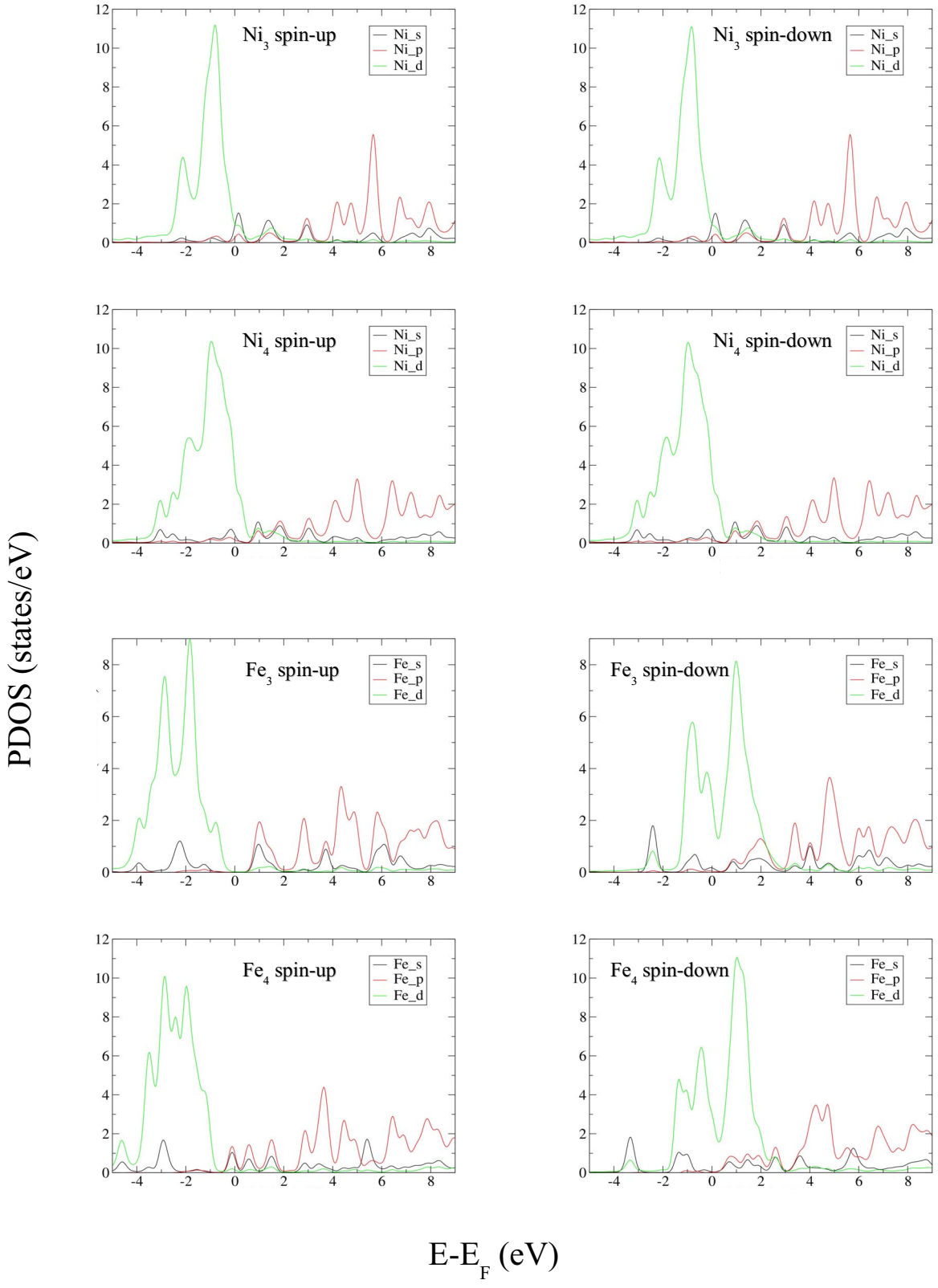

FIG. 6. (Color online) Ni and Fe PDOS of Ni_n(CHS-ZZC)/Ferro-A and Fe_n(CHS-ZZC)/Ferro-F (n=3,4) after full relaxation. The PDOS delta functions have been replaced by Gaussian functions of finite breadth.

Fe_3(CHS-ZZC)/Ferro-F, Fe_4(CHS-ZZC)/Ferro-F, and Fe_4(SEAS-ZZC)/Ferro-F, respectively; for other results, see the supplementary material.[57]

The geometries of Ni_3 and Ni_4 CHS-LCs and of Ni_3 CHS-ZZCs were hardly altered by relaxation, but in Ni_4 CHS-ZZCs the Ni atoms moved to bridge sites defining a rhom-

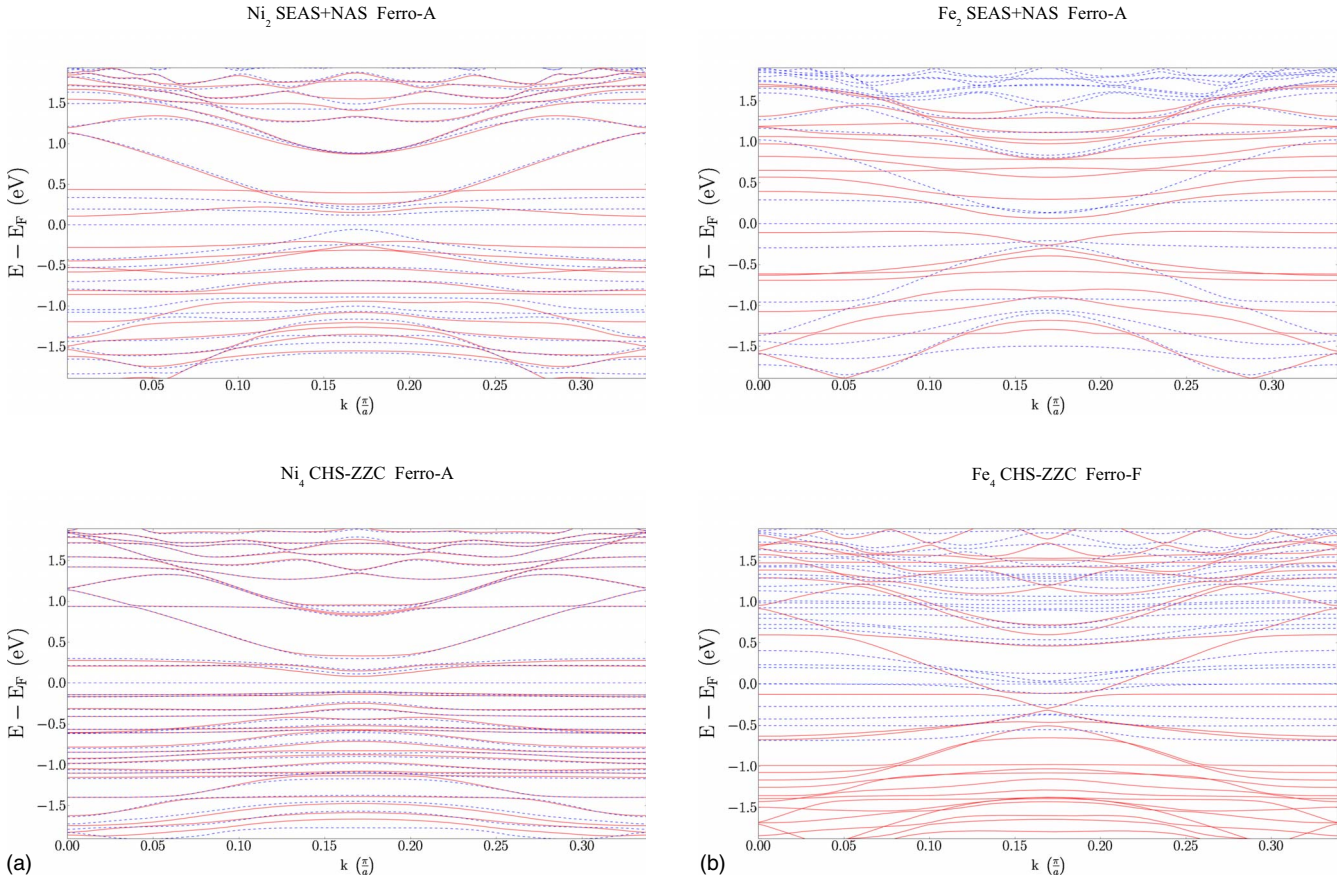

FIG. 7. (Color online) Electronic band structures of (a) Ni_2(SEAS+NAS)/Ferro-A and Ni_4(CHS-ZZC)/Ferro-A and (b) Fe_2(SEAS+NAS)/Ferro-A and Fe_4(CHS-ZZC)/Ferro-F. Continuous red lines correspond to spin-up bands; dashed blue lines correspond to spin-down bands.

boid corresponding approximately to a graphene unit cell. CHS-ZZCs were more stable than CHS-LCs, and, in keeping with the results for Ni/GNR and Ni_2/GNR, Ferro-A was more stable than Ferro-F.

Like their Ni analogs, Fe_3 and Fe_4 CHS-LCs retained their structures upon relaxation, and like their centrally located Fe and Fe_2 homologs were more stable as Ferro-F than as Ferro-A. Ferro-F was also the more stable GNR configuration in Fe_3 and Fe_4 ZZCs, but the Fe atoms of these ZZCs adopted geometries that were similar to the triangle and tetrahedron of free-standing Fe_3 and Fe_4 clusters, with one or more atoms separated from the GNR. For example, the bond lengths in Fe_3(CHS-ZZC)/Ferro-F [Fig. 4(a)] were 2.27, 2.28, and 2.30 Å, and its atomic spin magnetic moments were $2.8\mu_B$, $3.0\mu_B$, and $2.8\mu_B$ (Table II; cf. 2.12, 2.40, and 2.40 Å and $3.14\mu_B$, $3.15\mu_B$, and $3.70\mu_B$ for free-standing Fe_3 as predicted by SIESTA/GGA calculations); the bond lengths and atomic spin magnetic moments of Fe_4(CHS-ZZC)/Ferro-F [Fig. 4(b)] were 2.35, 2.35, 2.36, 2.38, 2.39, and 2.52 Å and $3.35\mu_B$, $2.87\mu_B$, $2.88\mu_B$, and $3.30\mu_B$, respectively [Table II; cf. 4×2.31 and 2×2.66 Å and $(4\times3.50)\mu_B$ for free-standing Fe_4]. Similar distorsions were observed in Fe_3(SEAS-ZZC)/Ferro-F and Fe_4(SEAS-ZZC)/Ferro-F (Fig. 5), which were more stable than their CHS-ZZC and CHS-LC analogs and had atomic spin magnetic moments even closer to those of the free-standing clusters. Thus the geometries of the most stable Fe_3/GNR and Fe_4/GNR structures that were investigated were not imposed by the planar geometry of the GNR but by those of the free Fe clusters, which underlines the weakness of the Fe-GNR interactions in comparison with the Fe-Fe interaction. That the atomic spin magnetic moments are so much larger in the Fe nanostructures than in their Ni analogs is attributable to the former, but not the latter, having a large excess of spin-down *d*-type states above E_F, as is illustrated in Fig. 6 by the cases of Ni_n(CHS-ZZC)/Ferro-A and Fe_n(CHS-ZZC)/Ferro-F ($n=3,4$).

As was indicated in Sec. I, the carbon atoms of each edge of a hydrogen-passivated zigzag GNR all have the same spin, and the GNR is metallic or semiconducting depending on whether the spins at the two edges are parallel (Ferro-F) or antiparallel (Ferro-A).[24] In both cases, there are flat energy bands near E_F that correspond to the π and π^* orbitals of the edge atoms. After computing the electronic band structure of Ni/GNR systems with the Ni atom at various different adsorption sites, Rigo *et al.*[29] reported that the electronic character of the GNR is not altered by adsorption of a single Ni atom, although its presence does perturb the energy bands. In this study we found that the same holds when two, three, or four Ni or Fe atoms are adsorbed, at least when the initial adsorption configurations are as in this study, as is shown in Figs. 7(a) and 7(b) for the cases

of Ni_2(SEAS+NAS)/Ferro-A, Ni_4(CHS-ZZC)/Ferro-A, Fe_2(SEAS+NAS)/Ferro-A, and Fe_4(CHS-ZZC)/Ferro-F. Note that, as is expected given the computed PDOS [see Fig. 6 for the cases of Ni_4(CHS-ZZC)/Ferro-A and Fe_4(CHS-ZZC)/Ferro-F], the Fe_n/GNR systems show more splitting indicative of interaction between spin-up and spin-down bands and that the flat sections of the energy bands near E_F in Ni_n/Ferro-A configurations extend to higher wave numbers as the number of adatoms increases, at the same time slightly reducing the gap between the states above and below E_F.

IV. SUMMARY AND CONCLUSIONS

In this work, using the computational package SIESTA[46] with standard nonlocal norm-conserving pseudopotentials[49] and the GGA to exchange and correlation,[48] we performed extensive *ab initio* DFT calculations to investigate the structural, magnetic, and electronic properties of Ni_n and Fe_n nanostructures ($n=1-4$) that were adsorbed on hydrogen-passivated $\langle 10,0\rangle$ zigzag GNRs. Ni_n clusters were more strongly bound than Fe_n clusters, and their atoms had much smaller spin magnetic moments. The difference in binding energies also explains why zigzag Ni_3 and Ni_4 chains placed at GNR hole sites retained close contact with the GNR upon relaxation, whereas the analogous Fe chains adopted geometries similar to those of free-standing Fe clusters, with one or more atoms lifted away from the GNR. An extensive study of adsorbed dimers shows that although, for both Ni_2 and Fe_2, the perpendicular DD-CHS and DD-SEAS configurations are, respectively, more stable than the epitaxial CHS+NHS and SEAS+NAS configurations, the most stable configurations of the dimers are those with the two atoms at adjoining SEASs. Like the pristine GNR, Ni_n/GNR systems were more stable in Ferro-A than in Ferro-F configuration, whereas among Fe_n/GNR systems this was only found for one- or two-atom adstructures at subedge or near-subedge atop sites. The conductivity type of the GNR (metallic in Ferro-F configuration, semiconducting in Ferro-A configuration) was unaltered by adsorption of up to four Ni or Fe atoms.

The results presented in this paper show that, as in other TM/all-carbon systems,[3,32–41,51–53] the structural, magnetic, and electronic properties of TM/GNR systems depend to a large extent on the nature of the TM atom. Accordingly, further simulations, as well as theoretical and experimental work, will be necessary for satisfactory understanding of the behavior of TM/GNR systems in general.

ACKNOWLEDGMENTS

This work was supported by the Spanish Ministry of Science and Innovation in conjunction with the European Regional Development Fund (Grant No. FIS2008-04894/FIS) and by the Directorate General for R+D+i of the Xunta de Galicia (Grants No. INCITE09E2R206033ES and No. INCITE08PXIB206107PR). J.C. thanks the Spanish Ministry of Education for an FPU grant. Facilities provided by the Galician Supercomputing Centre (CESGA) are also acknowledged.

[1] H. W. Kroto, J. R. Heath, S. C. O'Brien, R. F. Curl, and R. E. Smalley, Nature (London) **318**, 162 (1985).
[2] S. Iijima, Nature (London) **354**, 56 (1991).
[3] R. Saito, G. Dresselhaus, and M. S. Dresselhaus, *Physical Properties of Carbon Nanotubes* (Imperial, London, 1998).
[4] K. S. Novoselov, A. K. Geim, S. V. Morozov, D. Jiang, Y. Zhang, S. V. Dubonos, I. V. Grigorieva, and A. A. Firsov, Science **306**, 666 (2004).
[5] K. S. Novoselov, A. K. Geim, S. V. Morozov, D. Jiang, M. I. Katsnelson, I. V. Grigorieva, S. V. Dubonos, and A. A. Firsov, Nature (London) **438**, 197 (2005).
[6] Y. B. Zhang, Y.-W. Tan, H. L. Stormer, and P. Kim, Nature (London) **438**, 201 (2005).
[7] K. S. Novoselov, D. Jiang, F. Schedin, T. J. Booth, V. V. Khotkevich, S. V. Morozov, and A. K. Geim, Proc. Natl. Acad. Sci. U.S.A. **102**, 10451 (2005).
[8] S. Stankovich, D. A. Dikin, G. H. B. Dommett, K. M. Kohlhaas, E. J. Zimney, E. A. Stach, R. D. Piner, S. T. Nguyen, and R. S. Ruoff, Nature (London) **442**, 282 (2006).
[9] A. H. Castro Neto, F. Guinea, N. M. R. Peres, K. S. Novoselov, and A. K. Geim, Rev. Mod. Phys. **81**, 109 (2009).
[10] L. G. Cançado, M. A. Pimenta, B. R. A. Neves, G. Medeiros-Ribeiro, T. Enoki, Y. Kobayashi, K. Takai, K. Fukui, M. S. Dresselhaus, R. Saito, and A. Jorio, Phys. Rev. Lett. **93**, 047403 (2004).
[11] H. Lee, Y.-W. Son, N. Park, S. Han, and J. Yu, Phys. Rev. B **72**, 174431 (2005).
[12] Y.-W. Son, M. L. Cohen, and S. G. Louie, Phys. Rev. Lett. **97**, 216803 (2006).
[13] Y.-W. Son, M. L. Cohen, and S. G. Louie, Nature (London) **444**, 347 (2006).
[14] V. Barone, O. Hod, and G. E. Scuseria, Nano Lett. **6**, 2748 (2006).
[15] N. M. R. Peres, F. Guinea, and A. H. Castro Neto, Phys. Rev. B **73**, 125411 (2006).
[16] L. Brey and H. A. Fertig, Phys. Rev. B **73**, 235411 (2006).
[17] L. Pisani, J. A. Chan, B. Montanari, and N. M. Harrison, Phys. Rev. B **75**, 064418 (2007).
[18] T. Enoki, Y. Kobayashi, and K. I. Fukui, Int. Rev. Phys. Chem. **26**, 609 (2007).
[19] A. K. Geim and K. S. Novoselov, Nature Mater. **6**, 183 (2007).
[20] M. Y. Han, B. Özyilmaz, Y. Zhang, and P. Kim, Phys. Rev. Lett. **98**, 206805 (2007).
[21] B. Özyilmaz, P. Jarillo-Herrero, D. Efetov, D. A. Abanin, L. S. Levitov, and P. Kim, Phys. Rev. Lett. **99**, 166804 (2007).
[22] L. Yang, C.-H. Park, Y.-W. Son, M. L. Cohen, and S. G. Louie, Phys. Rev. Lett. **99**, 186801 (2007).
[23] O. Hod, V. Barone, J. E. Peralta, and G. E. Scuseria, Nano Lett. **7**, 2295 (2007).
[24] T. B. Martins, R. H. Miwa, A. J. R. da Silva, and A. Fazzio,

Phys. Rev. Lett. **98**, 196803 (2007).
[25] X. L. Li, X. R. Wang, L. Zhang, S. W. Lee, and H. J. Dai, Science **319**, 1229 (2008).
[26] J. Fernández-Rossier, Phys. Rev. B **77**, 075430 (2008).
[27] J. J. Palacios, J. Fernández-Rossier, and L. Brey, Phys. Rev. B **77**, 195428 (2008).
[28] F. Muñoz-Rojas, J. Fernández-Rossier, and J. J. Palacios, Phys. Rev. Lett. **102**, 136810 (2009).
[29] V. A. Rigo, T. B. Martins, A. J. R. da Silva, A. Fazzio, and R. H. Miwa, Phys. Rev. B **79**, 075435 (2009).
[30] D. V. Kosynkin, A. L. Higginbotham, A. Sinitskii, J. R. Lomeda, A. Dimiev, B. K. Price, and J. M. Tour, Nature (London) **458**, 872 (2009).
[31] L. Y. Jiao, L. Zhang, X. R. Wang, G. Diankov, and H. J. Dai, Nature (London) **458**, 877 (2009).
[32] A. Thess, R. Lee, P. Nikolaev, H. J. Dai, P. Petit, J. Robert, C. H. Xu, Y. H. Lee, S. G. Kim, A. G. Rinzler, D. T. Colbert, G. E. Scuseria, D. Tománek, J. E. Fischer, and R. E. Smalley, Science **273**, 483 (1996).
[33] Y. H. Lee, S. G. Kim, and D. Tománek, Phys. Rev. Lett. **78**, 2393 (1997).
[34] F. Banhart, N. Grobert, M. Terrones, J.-C. Charlier, and P. M. Ajayan, Int. J. Mod. Phys. B **15**, 4037 (2001).
[35] B. C. Guo, K. P. Kerns, and A. W. Castleman, Jr., Science **255**, 1411 (1992).
[36] B. C. Guo, S. Wei, J. Purnell, S. Buzza, and A. W. Castleman, Jr., Science **256**, 515 (1992).
[37] B. C. Guo and A. W. Castleman, Jr., in *Advances in Metal and Semiconductor Clusters*, edited by M. A. Duncan (JAI, London, 1994), Vol. 2, p. 137.
[38] J. S. Pilgrim and M. A. Duncan, J. Am. Chem. Soc. **115**, 6958 (1993).
[39] J. S. Pilgrim and M. A. Duncan, J. Am. Chem. Soc. **115**, 9724 (1993).
[40] L. S. Wang, X. B. Wang, H. B. Wu, and H. S. Cheng, J. Am. Chem. Soc. **120**, 6556 (1998).
[41] M.-M. Rohmer, M. Bénard, and J. M. Poblet, Chem. Rev. **100**, 495 (2000).
[42] A. N. Andriotis, M. Menon, and G. E. Froudakis, Phys. Rev. Lett. **85**, 3193 (2000).
[43] M. J. Frisch *et al.*, GAUSSIAN03, Revision D.01, Gaussian, Inc., Pittsburgh, PA, 2003.
[44] M. M. G. Alemany, O. Diéguez, C. Rey, and L. J. Gallego, J. Chem. Phys. **114**, 9371 (2001).
[45] H. Y. He, R. Pandey, and S. P. Karna, Chem. Phys. Lett. **439**, 110 (2007).
[46] J. M. Soler, E. Artacho, J. D. Gale, A. García, J. Junquera, P. Ordejón, and D. Sánchez-Portal, J. Phys.: Condens. Matter **14**, 2745 (2002).
[47] F. D. Novaes, A. J. R. da Silva, and A. Fazzio, Braz. J. Phys. **36**, 799 (2006).
[48] J. P. Perdew, K. Burke, and M. Ernzerhof, Phys. Rev. Lett. **77**, 3865 (1996).
[49] N. Troullier and J. L. Martins, Phys. Rev. B **43**, 1993 (1991).
[50] L. Kleinman and D. M. Bylander, Phys. Rev. Lett. **48**, 1425 (1982).
[51] C. Rey, M. M. G. Alemany, O. Diéguez, and L. J. Gallego, Phys. Rev. B **62**, 12640 (2000).
[52] R. C. Longo, M. M. G. Alemany, B. Fernández, and L. J. Gallego, Phys. Rev. B **68**, 167401 (2003).
[53] E. G. Noya, R. C. Longo, and L. J. Gallego, J. Chem. Phys. **119**, 11130 (2003).
[54] W. H. Press, S. A. Teukolsky, W. T. Vetterling, and B. P. Flannery, *Numerical Recipes in Fortran*, 2nd ed. (Cambridge University Press, Cambridge, 1992).
[55] M. Ezawa, Phys. Rev. B **73**, 045432 (2006).
[56] H. J. Monkhorst and J. D. Pack, Phys. Rev. B **13**, 5188 (1976).
[57] See supplementary material at http://link.aps.org/supplemental/10.1103/PhysRevB.81.115418 for the spin density distributions and spin magnetic moments of the other Ni_n/GNR and Fe_n/GNR systems ($n=1-4$) considered in this paper.
[58] H. Johll, H. C. Kang, and E. S. Tok, Phys. Rev. B **79**, 245416 (2009).
[59] A. Kokalj, Comput. Mater. Sci. **28**, 155 (2003). Code available from http://www.xcrysden.org/
[60] J. C. Tung and G. Y. Guo, Phys. Rev. B **76**, 094413 (2007).